



## 1 **Measurement report: Analysis of aerosol optical depth** 2 **variation at Zhongshan Station in Antarctica**

3 Lijing Chen<sup>1,2</sup>, Lei Zhang<sup>1</sup>, Yong She<sup>2</sup>, Zhaoliang Zeng<sup>1</sup>, Yu Zheng<sup>1</sup>, Biao Tian<sup>1</sup>,  
4 Wenqian Zhang<sup>1</sup>, Zhaohui Liu<sup>3</sup>, Minghu Ding<sup>\*1</sup>

5 <sup>1</sup> State Key Laboratory of Severe Weather, Chinese Academy of Meteorological Sciences, Beijing,  
6 100081, China.

7 <sup>2</sup> Chengdu University of Information Technology, Chengdu, 610103, China.

8 <sup>3</sup> Polar Surveying and Mapping Engineering Center of Heilongjiang Administration of Surveying,  
9 Mapping and Geoinformation, Harbin 150081, China

10 *Correspondence to:* Minghu Ding (dingminghu@foxmail.com)

11 Three key findings:

- 12 ● The AOD level over Zhongshan Station in Antarctica is low in summer and high in  
13 winter. AE indicates the dominance of fine (coarse) aerosols in summer (winter).
- 14 ● The increase in AOD during spring and winter correlates with a reduction in the fine  
15 mode fraction, whereas the increase observed in summer and autumn may be attributed  
16 to the growth and aging of fine particles.
- 17 ● AOD varied inversely with wind speed and showed an insignificant positive correlation with  
18 temperature but a significant negative correlation with relative humidity.

19 **Abstract:** Our understanding of aerosol optical depth (AOD) in Antarctica remains limited due to the  
20 scarcity of ground observation stations and limited daylight days. Utilizing data from the CE318-T  
21 photometer spanning from January 2020 to April 2023 at Zhongshan Station, we analysed the seasonal,  
22 monthly, and diurnal variations in AOD and Ångström exponent (AE). AOD median values increased  
23 from spring (0.033) to winter (0.115), while AE peaked during summer (1.010) and autumn (1.034),  
24 declining in winter (0.381), indicating a transition in dominant aerosol particle size from fine to coarse  
25 mode between summer and winter. Monthly mean AOD variation closely paralleled the proportion of  
26  $AE < 1$ , suggesting fluctuations in coarse mode particle proportions drive AOD variation. Increases in  
27 AOD during spring and winter correlated with decreases in fine mode fraction, while increases during  
28 summer and winter related to fine mode particle growth and aging. We observed a peak in AOD ( $\sim 0.06$ )  
29 at 14:00 local time at Zhongshan Station, possibly associated with a slight decrease in boundary layer



30 height (BLH). Additionally, higher (lower) wind speeds corresponded to lower (higher) AOD values,  
31 indicating the diffusion (accumulation) effect. The temperature and AOD showed an insignificant  
32 positive correlation between ( $R = 0.22$ ,  $p = 0.40$ ), relative humidity exhibited a significant negative  
33 correlation with AOD ( $R = -0.59$ ,  $p = 0.02$ ). Backward trajectory analysis revealed that coarse particles  
34 from the ocean predominantly contributed to high AOD daily mean values in summer, while fine  
35 particles on low AOD days originated mainly from the air mass over the Antarctic Plateau.

## 36 **1 Introduction**

37 Aerosols play an important role in impacting the climate system by absorbing and scattering solar  
38 radiation (Li et al., 2022). Antarctica, considered one of the most pristine lands, serves as an ideal  
39 background area for evaluating the climate effects of aerosols (Kamra, 2022). Marine aerosols emitted  
40 from the Southern Ocean are a primary source contributing to the aerosol load in the Antarctica (Thakur,  
41 2019). The retreat of sea ice in Antarctica is expected to escalate the release of sea salt and secondary  
42 biogenic aerosols (Yan et al., 2020). Sea salt particles with strong scattering may produce negative  
43 effective radiative forcing or indirect radiative effect by influencing cloud condensation nuclei within  
44 the marine boundary layer over Antarctica (Thornhill et al., 2021; Udisti et al., 2012). However, the  
45 heating effect of absorbent aerosols, such as black carbon (BC), may be amplified by the high surface  
46 albedo in Antarctica (Kang et al., 2020). In recent years, there has been a notable increase in BC  
47 concentrations in Antarctica, with BC deposition on snow and ice surfaces contributing to reduced  
48 surface albedo and increased solar radiation absorption, subsequently accelerating snow and ice melt  
49 (Kannemadugu et al., 2023). Given the close connection between aerosol radiation effects and their  
50 optical properties (Che et al., 2024), it is necessary to investigate the optical parameters of Antarctica  
51 aerosols.

52 Aerosol optical depth (AOD), as a key parameters of aerosol optical properties, serves as an effective  
53 measure of aerosol load and can influence the solar radiation components (Alghoul et al., 2009). AOD  
54 observation records from Antarctica sites indicate that the mean values range from 0.02 to 0.2 in coastal  
55 regions and from 0.005 to 0.03 in inland regions (Tomasi et al., 2007, 2012; Yang et al., 2021;  
56 Kannemadugu et al., 2023). Typically, coastal aerosols consist primarily of coarse-mode sea salt particles



57 during austral winter, while fine-mode particles (such as dimethyl sulfide and its oxidation product  
58 mesylate, DMS, and MSA) lead to elevated particle number concentrations in summer (20-100 times  
59 higher than in winter) (Shaw, 1979; Lachlan-Cope et al., 2020). Conversely, aerosols over the Antarctic  
60 Plateau predominantly comprise fine-mode particles of non-sea-salt sulfate (NSS) and DMS (Harder et  
61 al., 2000; Walters et al., 2019).

62 Additionally, particle size plays a significant role in aerosol extinction. The Ångström exponent (AE)  
63 serves as an important indicator of aerosol size, with value greater (less) than 1 indicating a predominance  
64 of fine (coarse) mode particles (Schuster et al., 2006). Weller and Lampert report that the mean AE at  
65 Neumayer Station was  $1.5 \pm 0.6$  and  $1.2 \pm 0.5$  during summer and winter, respectively, suggesting an  
66 increased contribution of fine-mode biological sulfate particles in summer (Weller and Lampert, 2008).  
67 Virkkula et al. observed higher scattering AE estimate values during summer ( $\sim 1.9$ ) and lower values  
68 during winter ( $\sim 0.8$ ) at Dome C on the Antarctic Plateau, indicating a prevalence of fine particles in  
69 summer (Virkkula et al., 2022).

70 Currently, the challenging environment and the limited number of daylight days per year restrict the  
71 availability of ground sites capable of obtaining adequate AOD and AE observations. Consequently, the  
72 optical properties of aerosols across large parts of Antarctica remain unexplored. To improve our  
73 comprehension of aerosol properties in Antarctica, we analyse the seasonal, monthly, and diurnal  
74 variations of AOD and AE using data obtained from the recently installed sun-sky-lunar CE318-T  
75 photometer at Zhongshan Station.

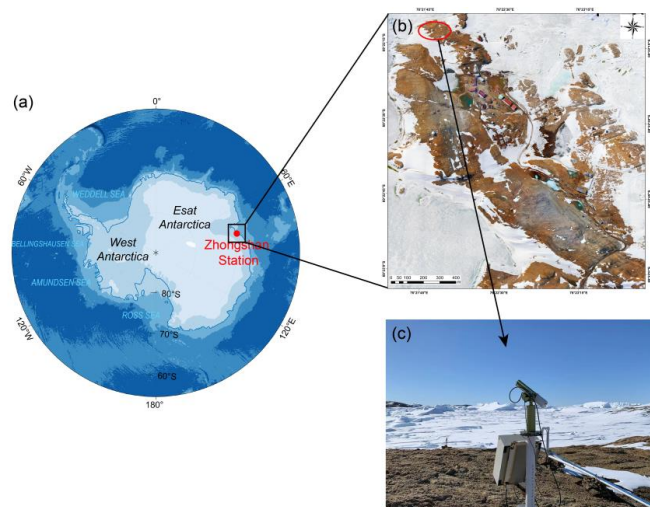
## 76 **2 Site, Instrument, and Data**

### 77 **2.1 Site Introduction**

78 Zhongshan Station ( $69^{\circ}22'12''\text{S}$ ,  $76^{\circ}21'49''\text{E}$ , 18 m a.s.l.) is located at the Larsemann Hills of Prydz Bay  
79 on the east Antarctic continent. The sun-sky-lunar CE318-T photometer is installed at Swan Ridge,  
80 northwest of the Nella fjord (Fig. 1) (Tian et al., 2022). This location experiences 54 polar days and 58  
81 polar nights annually, with snow covering the surrounding surface during winter and revealing bare rock  
82 in summer. In this study, the austral spring, summer, autumn, and winter are referred to the season from  
83 September to November (SON), December to February of next year (DJF), March to May (MAM), and



84 June to August (JJA), respectively. The average annual air temperature is  $-10\text{ }^{\circ}\text{C}$ , with a relative humidity  
85 of 58% and prevailing wind speeds of  $6.9\text{ m s}^{-1}$ , primarily from the east or east-southeast direction  
86 (Ding et al., 2022).



87  
88 **Figure 1 (a) The location of Zhongshan Station in Antarctica, (b) the aerial view of Zhongshan Station, and**  
89 **(c) the sun-sky-lunar photometer CE318-T at Zhongshan Station.**

## 90 2.2 Instrument and Data

91 The AOD measurement data utilized in this study were obtained from the sun-sky-lunar CE318-T  
92 photometer, manufactured by CIMEL Electronique, France. The CE318-T is a ground-based multiband  
93 radiometer capable of inverting aerosol optical parameters by measuring the spectral data of direct solar  
94 and lunar radiation extinction and the angular distribution of sky radiances (Barreto et al., 2016).  
95 We collected AOD level 1.5 (cloud-screened) data across various wavelengths spanning from January  
96 2020 to April 2023 (Fig. S1). However, the operation of CE318-T in polar environment is impeded by  
97 solar radiation and weather conditions, leading to a significant number of missing measurements.  
98 Consequently, we categorize daily observations with less than 20 measurements and the coefficient of  
99 dispersion (CV) exceeding 1 as invalid data, which are systematically eliminate from our analysis.  
100 Typically, these invalid data manifest with exceeding high AOD values, often attributed to instrument  
101 downtime caused by factors such as precipitation or cloudy weather. Moreover, to ensure the accuracy  
102 of AOD measurement at Zhongshan Station, we refine our data by cross-referencing station operation



103 records and the time series of black carbon (BC) concentrations. This process allows us to exclude AOD  
104 data associated with significant station activities and periods of elevated BC concentrations, thereby  
105 enhancing the reliability of our analysis.

106 The meteorology data, including temperature, relative humidity, wind direction, and wind speed, were  
107 obtained from the Zhongshan Station meteorology observatory, with the temporal resolution of 1 hour.

108 BLH data was obtained from ERA5 reanalysis provided by European Centre for Medium Range Weather  
109 Forecasts (ECMWF) with the temporal and spatial resolution of 1 hour and 0.25 (latitude) × 0.25  
110 (longitude).

111 The Hybrid Single-Particle Lagrangian Integrated Trajectory (HYSPLIT) model, is a comprehensive  
112 model developed by the National Oceanic and Atmospheric Administration (NOAA) and the Air  
113 Resources Laboratory (ARL) to calculate and analyse the source, transport, and diffusion trajectories of  
114 atmospheric pollutants. The meteorological data used in the HYSPLIT model comes from the National  
115 Center for Environmental Prediction (NCEP) Global Data Assimilation System (GDAS). In this study,  
116 the HYSPLIT model is utilized to calculate the 168h backward air mass trajectory from 3 altitudes of  
117 50,500 and 1000 m (amsl) to Zhongshan Station.

## 118 **3 Results**

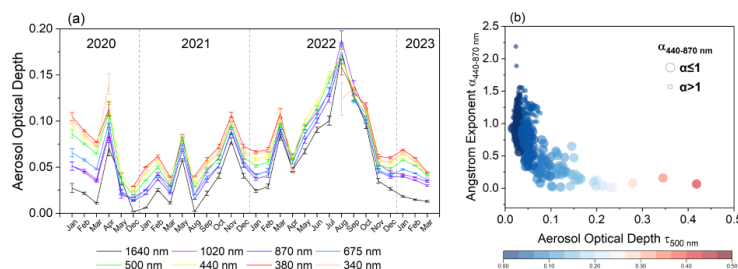
### 119 **3.1 Variation Characteristics of AOD**

120 From January 2020 to March 2023, the monthly mean AOD values at various wavelengths varied from  
121 0.00 to 0.20, with the lowest values in December 2020 and the highest values in August 2022 (Fig. 2a).

122 The monthly mean AOD values at 500 nm ( $AOD_{500\text{ nm}}$ ) generally remained below 0.1, consistent with  
123 findings by Gadhavi and Achuthan at the Maitri Station, where AOD variation fell within the range of  
124 0.01 to 0.10 (Gadhavi and Achuthan, 2004). The annual mean  $\pm$  SD (standard deviation) values of the  
125  $AOD_{500\text{ nm}}$  were  $0.074\pm 0.090$ ,  $0.051\pm 0.066$ ,  $0.071\pm 0.117$ , and  $0.053\pm 0.031$  in 2020, 2021, 2022, and  
126 2023, respectively (Table 1). The annual mean  $\pm$  SD values of the  $AE_{440-870\text{ nm}}$  were  $1.134\pm 0.411$ ,  
127  $0.953\pm 0.338$ ,  $0.883\pm 0.374$ ,  $0.753\pm 0.206$  in 2020, 2021, 2022, and 2023, which suggests that the  
128 aerosols over Zhongshan Station were mainly dominated by fine mode particles in 2020, and coarse  
129 mode particles in 2021, 2022, and 2023, respectively. The relationship between multi-year  $AOD_{500\text{ nm}}$



130 and  $AE_{440-870\text{ nm}}$  illustrates that fine mode particles are primarily concentrated in the range of  $AOD_{500\text{ nm}}$   
 131  $< 0.1$ , while high  $AOD_{500\text{ nm}}$  values, which occur occasionally, are caused by coarse mode particles (Fig.  
 132 2b).



133  
 134 **Figure 2 (a) Monthly variation of mean aerosol optical depth at different wavelengths measured over**  
 135 **Zhongshan Station in Antarctica from 2020 to 2023. (b) Relationship between  $AOD_{500\text{ nm}}$  and  $AE_{440-870\text{ nm}}$  over**  
 136 **Zhongshan Station from 2020 to 2023.**

137 **Table 1 Annual mean and standard deviation of aerosol optical depth at different wavelengths and Angstrom**  
 138 **Exponent at 440-870 nm at Zhongshan Station from 2020 to 2023.**

	2020	2021	2022	2023
$AOD_{1640\text{ nm}}$	$0.02811 \pm 0.10243$	$0.02639 \pm 0.07887$	$0.04989 \pm 0.14113$	$0.01604 \pm 0.03631$
$AOD_{1020\text{ nm}}$	$0.04898 \pm 0.09501$	$0.04519 \pm 0.0728$	$0.06709 \pm 0.13069$	$0.03965 \pm 0.0337$
$AOD_{870\text{ nm}}$	$0.04659 \pm 0.09314$	$0.03901 \pm 0.07044$	$0.06033 \pm 0.1264$	$0.03669 \pm 0.03244$
$AOD_{675\text{ nm}}$	$0.05887 \pm 0.09128$	$0.04224 \pm 0.06786$	$0.06339 \pm 0.12164$	$0.04407 \pm 0.03139$
$AOD_{500\text{ nm}}$	$0.07431 \pm 0.08972$	$0.05083 \pm 0.06557$	$0.07108 \pm 0.1173$	$0.05288 \pm 0.03091$
$AOD_{440\text{ nm}}$	$0.08093 \pm 0.08902$	$0.05744 \pm 0.0648$	$0.07715 \pm 0.11592$	$0.0574 \pm 0.03106$
$AOD_{380\text{ nm}}$	$0.08854 \pm 0.09143$	$0.06302 \pm 0.06542$	$0.07699 \pm 0.11697$	$0.0613 \pm 0.03169$
$AOD_{340\text{ nm}}$	$0.08758 \pm 0.09536$	$0.05881 \pm 0.06431$	$0.0732 \pm 0.11763$	$0.05831 \pm 0.03242$
$AE_{440-870\text{ nm}}$	$1.13411 \pm 0.41069$	$0.95284 \pm 0.33823$	$0.88293 \pm 0.3738$	$0.75257 \pm 0.20645$

139

### 140 0363.2 Seasonal and Monthly Variations in AOD and Ångström Exponent

141 The seasonal variation of  $AOD_{500\text{ nm}}$  and  $AE_{440-870\text{ nm}}$  over Zhongshan Station suggests the median  $AOD_{500}$   
 142  $\text{nm}$  values are lower in spring (0.033), summer (0.036), and autumn (0.045), but higher in winter (0.115),  
 143 while the  $AE_{440-870\text{ nm}}$  values are 0.908, 1.010, 1.036, and 0.381, respectively (Fig. 3a). The frequency



144 histograms show that the highest frequency range of  $AOD_{500\text{ nm}}$  is 0.02 to 0.04 in spring, summer, and  
145 autumn, while 0.08 to 0.12 in winter (Fig. S2). The normal fitting curves of the frequency histograms of  
146  $AE_{440-870\text{ nm}}$  indicate that the peak in winter is in the low-value range (0.3~0.4), while the peaks in spring,  
147 summer, and autumn are in the high-value range (1.0~1.2).

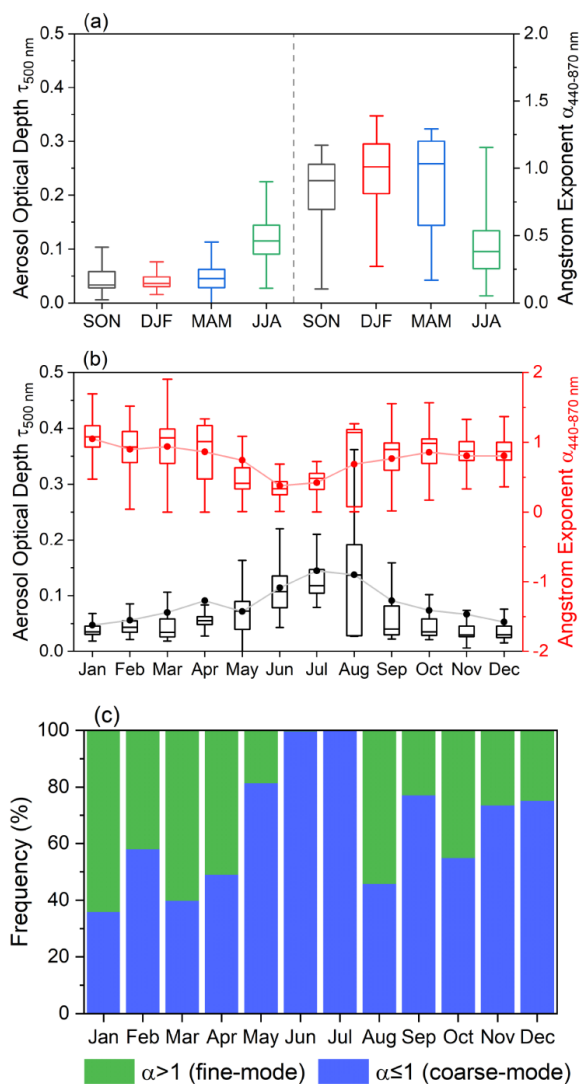
148 The seasonal variations in AOD and AE are consistent with previous findings on sea salt aerosol  
149 concentrations, although the mechanism behind this seasonal variation is multifaceted. Wang and Huang  
150 et al. have indicated that higher winter wind speeds at Zhongshan Station can elevate marine source  
151 aerosol concentrations, primarily composed of sea salt, potentially explaining the winter peak in sea salt  
152 concentration (Hong et al., 2009; Huang et al., 2005). However, Hall and Wolff propose that the high  
153 sea salt load correlates more with moderate wind speeds and shifts in wind direction, rather than high  
154 wind speeds, with concentrated brine on freshly formed ice surfaces acting as a source of winter sea salt  
155 (Hall and Wolff, 1998). Moreover, blowing snow over sea ice generates aerosols primarily made of sea  
156 salt, contributing to the winter peak in sea salt aerosols (Frey et al., 2020). Low sea salt concentrations  
157 in summer determined lower AOD levels, and the higher AE indicates a dominance of smaller particle  
158 sizes. In the marine boundary layer over the eastern Southern Ocean sector,  $nssSO_4^{2-}$  and MSA  
159 contribute approximately 40% of the total mass of fine aerosols (particle size  $< 0.56\ \mu\text{m}$ ) (Xu et al.,  
160 2021). Xu et al. reported the annual mean concentrations of  $nssSO_4^{2-}$  and MSA at Zhongshan Station  
161 were  $0\text{--}79\ \text{ng m}^{-3}$  and  $19\text{--}41\ \text{ng m}^{-3}$ , respectively, with the maximum concentrations were observed  
162 in summer (Xu et al., 2019). This increase in summer concentrations is attributed to enhanced solar  
163 radiation, phytoplankton blooms in the polynyas releasing DMS (Zhang et al., 2015), and the DMS in  
164 the atmosphere is oxidized by radicals such as  $O_3$  (significant at high latitudes), OH, and BrO in the gas  
165 phase (Boucher et al., 2003), resulting in elevated concentrations of MSA and  $nssSO_4^{2-}$ . The positive  
166 correlation between mean surface chlorophyll and AOD in the Southern Ocean confirmed the  
167 contribution of DMS flux to aerosol load during summer (Gabric et al., 2005).

168 The monthly variations in  $AOD_{500\text{ nm}}$  and  $AE_{440-870\text{ nm}}$  at Zhongshan Station suggest an opposite trend,  
169 with the mean values of  $AOD_{500\text{ nm}}$  peaking in July and  $AE_{440-870\text{ nm}}$  reaching its lowest in June (Fig. 3b).  
170 Median  $AOD_{500\text{ nm}}$  values increase slightly from January to February, followed by a decrease in March  
171 and increase continuously from March to August, reach the maximum value, then gradually decrease,



172 and reach the minimum in November and December. The percentages of  $AE_{440-870\text{ nm}} > 1.0$  and  $AE_{440-8870}$   
173  $_{\text{nm}} < 1.0$  represent the proportion of the monthly occurrence frequency of fine and coarse mode particles  
174 (Fig. 3c). The monthly mean and median  $AOD_{500\text{ nm}}$  values are consistent with the proportion of coarse  
175 mode particles ( $AE_{440-870\text{ nm}} > 1.0$ ), suggesting that the variation characteristics of  $AOD_{500\text{ nm}}$  at  
176 Zhongshan Station are primarily influenced by coarse mode particles. Given that Zhongshan Station is  
177 located in the coastal area of Antarctica, it is suspected that these coarse particles may be sea salt aerosols.





178

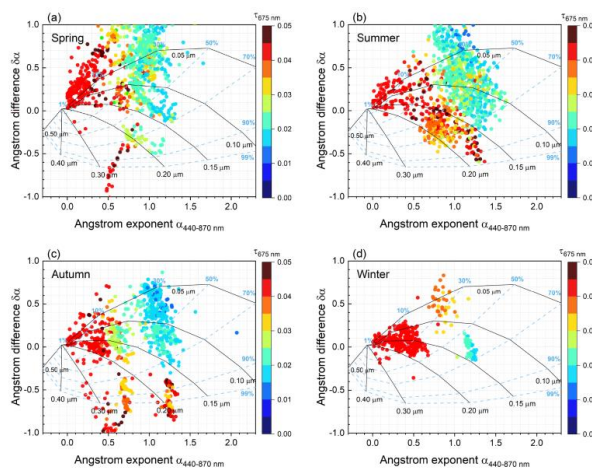
179 **Figure 3** (a) Seasonal variation of aerosol optical depth at 500 nm and Angstrom exponent at 440-870 nm over  
 180 Zhongshan Station. For each monthly box, the central line indicates the median; and the bottom and top edges  
 181 of the box indicate the 25th and 75th percentiles, respectively. (b) Variations in monthly AOD<sub>500 nm</sub> and AE<sub>440-</sub>  
 182 <sub>870 nm</sub> at Zhongshan Station. For each monthly box, the central line indicates the median; the dot represents  
 183 the mean; and the bottom and top edges of the box indicate the 25th and 75th percentiles, respectively. (c)  
 184 Monthly percentages of Ångström exponent >1.0 (green) and Ångström exponent ≤ 1.0 (blue) at Zhongshan  
 185 Station from 2020 to 2023.

186 Additionally, we used a graphical method proposed by Gobbi et al (Gobbi et al., 2007), which is based  
 187 on Mie calculation and correlates Ångström exponent ( $\alpha$ ) and Ångström exponent spectral difference



188 ( $\delta\alpha$ ) with fine mode aerosol effective radius ( $R_{eff}$ ) and fine mode fraction to investigate the aerosol  
189 modification processes at Zhongshan Station in different seasons. Figure 4 presents a schematic diagram  
190 of the classification of aerosol types using the  $\alpha$  and  $\delta\alpha$  functions of a dual-mode, lognormal  
191 distribution with refractive index =  $1.4 - 0.001i$  as reference. It is known from Jurányi and Weller'  
192 research that the refractive index of Antarctic coastal aerosol is about 1.4, so it seems reasonable to use  
193 this reference (Jurányi and Weller, 2019). We utilized  $AOD_{440nm}$ ,  $AOD_{675nm}$ , and  $AOD_{870nm}$  to calculate  
194  $\alpha_{440-675nm}$ ,  $\alpha_{440-870nm}$ , and  $\alpha_{675-870nm}$ , and then get the  $\delta\alpha = \alpha_{440-675nm} - \alpha_{675-870nm}$ . The  
195 negative values of  $\delta\alpha$  indicate the dominance of fine mode aerosol, while positive values indicate the  
196 effect of two separate particle modes (Kaufman, 1993). The solid black line represents the size of fine  
197 mode particles, and the dashed blue line represents the proportion of the contribution of fine mode  
198 particles to AOD. In Fig. 4, increasing  $AOD_{675nm}$  is associated with the declining  $\eta$  (spring and winter)  
199 and increasing  $R_{eff}$  (summer and autumn). This indicates that higher aerosol loads in spring and winter  
200 are attributed to increased coarse-mode particle fractions, whereas in summer and autumn are primarily  
201 associated with the increase of fine-mode particle size. Previous studies have indicated that sea salt  
202 dominates winter aerosols in the coastal areas of Antarctica (Hall and Wolff, 1998; Weller et al., 2008),  
203 and Xu et al observed that the highest mean concentration of sea salt in September at Zhongshan Station,  
204 these can explain the  $\delta\alpha$  values are mainly positive in spring and winter, and  $\eta$  is concentrated within  
205 the range of less than 50% (Xu et al., 2019). In summer and autumn, apart from common sea salt aerosols  
206 ( $\delta\alpha > 0$ ,  $\eta < 50$ ), the high AOD is mainly related to the particle growth such as hygroscopic growth or  
207 condensation of fine mode aerosols ( $R_{eff}: 0.10\mu m \sim 0.20\mu m$ ). This may be linked to the atmospheric  
208 oxidation of (DMS) emitted by biological sources in coastal regions, or the aging process of aerosols  
209 originating from other sources, as the rate of new particle formation and particulate matter growth in  
210 summer is much greater than in winter in the Antarctica (Davison et al., 1996; Weller et al., 2015;  
211 Lachlan-Cope et al., 2020).

212



213

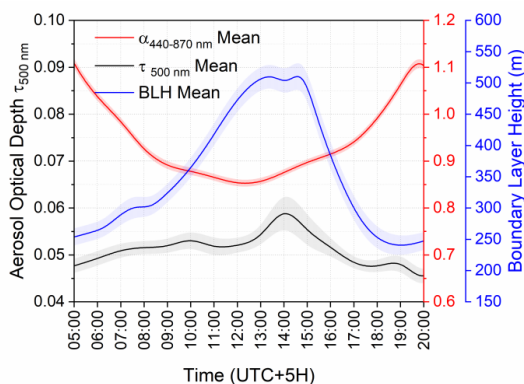
214 **Figure 4** Ångström exponent difference ( $\delta\alpha = \alpha_{440-675\text{ nm}} - \alpha_{675-870\text{ nm}}$ ) as a function of the  $\alpha_{440-870\text{ nm}}$   
 215 and  $AOD_{675\text{ nm}}$  (colour scale) during (a) spring, (b) summer, (c) autumn, and (d) winter at Zhongshan Station.  
 216 The black lines indicate the  $R_{eff}$  of fine-mode aerosols, while the blue lines correspond to fine-mode fraction  
 217 ( $\eta$ ).

### 218 3.3 Relationship between AOD, Ångström Exponent and Meteorological Conditions

219 In this section, we analyse the diurnal variation characteristics of  $AOD_{500\text{ nm}}$  and  $AE_{440-870\text{ nm}}$  during  
 220 summer and explore their correlation with meteorological variables within the planetary boundary layer  
 221 (PBL), such as wind directions and speeds, temperature, and relative humidity. We calculated the diurnal  
 222 variations of  $AOD_{500\text{ nm}}$  and  $AE_{440-870\text{ nm}}$  based on observations collected at Zhongshan Station during  
 223 summer (December-February, 2020-2023), with each hourly mean containing at least one thousand  
 224 individual observations (Fig. 5Figure 5). The mean  $AOD_{500\text{ nm}}$  exhibited an increase from 5:00 to 14:00  
 225 (local time of Zhongshan Station), reaching a maximum value ( $0.06 \pm 0.04$ ), and then decreased. The  
 226 mean  $AE_{440-870\text{ nm}}$  decreased from 5:00 to 12:00 to the lowest value ( $0.85 \pm 0.25$ ) and then increased. These  
 227 results indicate that the highest aerosol load occurs at 14:00, accompanied by a larger aerosol particle  
 228 size during this period. The diurnal variation of boundary layer height (BLH) is almost consistent with  
 229 the variation of  $AOD_{500\text{ nm}}$ , which is inconsistent with the general conclusion that the negative correlation  
 230 between BLH and particulate matter concentration in the mid-latitudes (Miao and Liu, 2019; Lou et al.,  
 231 2019). However, a minor decline in BLH is noticeable when the  $AOD_{500\text{ nm}}$  value reaches its peak at  
 232 14:00. Consequently, we suspect that the weak absorption and low content of Antarctic aerosols typically

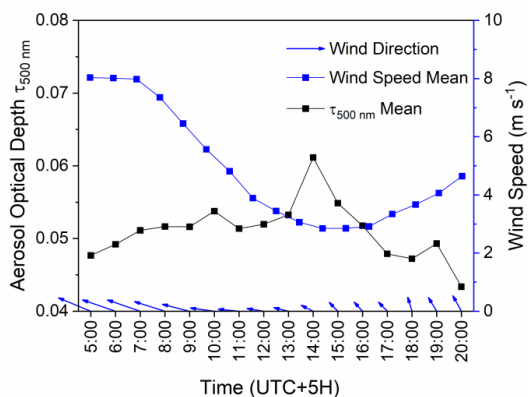


233 do not suffice to form an “aerosol-boundary layer” positive feedback mechanism, but may contribute to  
234 reducing the BLH when AOD is high (Petäjä et al., 2016; Lou et al., 2019).



235  
236 **Figure 5 Diurnal variation of AOD<sub>500 nm</sub> and AE<sub>440-870 nm</sub> at Zhongshan Station. The black line indicates the**  
237 **mean of AOD<sub>500 nm</sub>; the red line represents the mean of AE<sub>440-870 nm</sub>; the blue line represents the mean of BLH.**  
238 **The shadow represents the standard deviation of the mean.**

239 Moreover, the diurnal variation of the 2-minute wind at Zhongshan Station reveals prevailing southeast  
240 direction, with average speeds range from 2 to 9 m s<sup>-1</sup>. There is a noticeable decline in wind speeds  
241 between 5:00 and 14:00, followed by a gradual increase thereafter (Fig. 6). Given that the CE318-T is  
242 positioned westward of the main Zhongshan Station building, the eastward winds may carry emissions  
243 originating from western stations such as Zhongshan and Progress Station. The relationship between the  
244 diurnal variation of AOD<sub>500 nm</sub> and wind speed is more obvious: AOD<sub>500 nm</sub> exhibits a decline (increase)  
245 concurrent with decreasing (increasing) wind speeds. This correlation stems from the fact that higher  
246 wind speeds facilitate the dispersion of pollutants, leading to a reduction in AOD, and vice versa (Liu et  
247 al., 2020; Coccia, 2021; Wang et al., 2022).



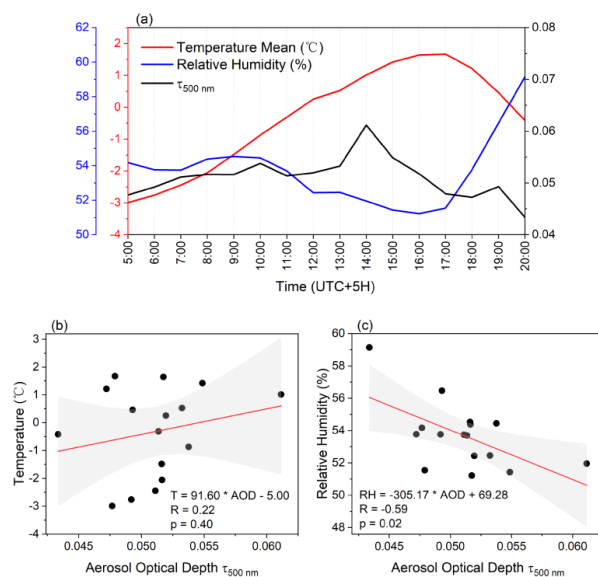
248

249 **Figure 6 Diurnal variations of 2-minute wind direction and speed, and AOD<sub>500 nm</sub> in summer at Zhongshan**  
 250 **Station.**

251 The influence of temperature and relative humidity on aerosol parameters is relatively complex.  
 252 Temperature affects aerosol particle concentration by influencing the air convection and influences the  
 253 formation and optical properties of secondary by controlling chemical transformation (Li et al., 2020;  
 254 Han et al., 2007). Relative humidity affects the chemical composition, size distribution, and optical  
 255 properties of aerosol particles by affecting their aqueous-phase reactions and gas-particle partitioning  
 256 (Sun et al., 2013; Altieri et al., 2008; Ding et al., 2021; Hennigan et al., 2008). The diurnal variations of  
 257 AOD<sub>500 nm</sub>, temperature, and relative humidity in summer at Zhongshan Station show that AOD<sub>500 nm</sub> is  
 258 positively correlated with temperature with a correlation coefficient of 0.22, and AOD<sub>500 nm</sub> is negatively  
 259 correlated with relative humidity with a correlation coefficient of -0.59 (Fig. 7). This indicates that rising  
 260 (declining) temperature and declining (rising) relative humidity during the day may contribute to an  
 261 increase (declining) in aerosol load. Previous studies have shown a positive correlation between  
 262 temperature and AOD (Basharat et al., 2023). During the summer at Zhongshan Station, high  
 263 temperatures may destroy the physical properties of bare rocks and promote the formation and diffusion  
 264 of particulate matter, thereby increasing the aerosol load (Zhang, 2024). However, there is a study  
 265 showing that higher temperatures may reduce methane sulfinic acid (MSIA) yield (Cecilia Arsene et al.,  
 266 1999). Therefore, the effect of temperature on the AOD at Zhongshan Station is complex, resulting in an  
 267 insignificant positive correlation. The relationship between relative humidity and AOD is inconclusive  
 268 (Gautam et al., 2022), as high relative humidity may contribute to the increase of aerosol hygroscopic  
 269 properties leading to an increase in AOD (Meng et al., 2024), or it may contribute to a decrease in AOD



270 by reducing dust particles in the air (Zhang, 2024). Therefore, the influence of temperature and relative  
 271 humidity on AOD may be related to the physicochemical properties of local aerosols and their sourcing  
 272 and sink processes.



273  
 274 **Figure 7 (a) Diurnal variations of AOD<sub>500 nm</sub> (black), temperature (red), and relative humidity (blue) in**  
 275 **summer at Zhongshan Station; (b) relationship between AOD<sub>500 nm</sub> and temperature; and (c) relationship**  
 276 **between AOD<sub>500 nm</sub> and relative humidity. The red line indicates the regression line obtained by fitting a linear**  
 277 **regression, and the grey bands indicate the confidence intervals for the linear regression.**

#### 278 4 Discussion

279 In addition to meteorological conditions that can affect the diurnal variation characteristics of AOD, we  
 280 believe that aerosol sources may be another influencing factor. We classified days with mean AOD below  
 281 the 5th percentile as low AOD day and those above the 95th percentile as high AOD day (Fig. S3 and  
 282 Table S1). Using the HYSPLIT backward trajectory model, we found that air masses on high AOD days  
 283 primarily originated from the ocean, whereas those on low AOD days mostly came from the interior of  
 284 Antarctica (Fig. S4). The altitudes of the backward trajectories show that during low AOD days, the air  
 285 mass originating from the ocean usually starts at a lower altitude (<1000 m), rises to a higher altitude  
 286 (~2000 m) and then descends to Zhongshan Station (2020-05-15 and 2020-12-25), while the air mass  
 287 originating from the interior of Antarctica usually starts at a higher altitude (~3000 m) and then descends



288 to Zhongshan Station. This indicates that particles from the Antarctic plateau or the free troposphere  
289 above the Antarctic interior are transported to Zhongshan Station by katabatic winds. Researches show  
290 that the katabatic winds driven by latent cooling occurring in the high-wind East Antarctic can rush the  
291 dense air from the interior plateau to the coast (Yu et al., 2020; Simmons et al., 2021). Combined with  
292 the AE values, we can find that the AE values of low AOD days are usually greater than 1, indicating  
293 the small particle size, thus, we suspect that these fine particles may be  $nssSO_4^{2-}$  from the Antarctic  
294 interior (Pei et al., 2021). In contrast, in high AOD days, the air mass all originates in the ocean and  
295 usually starts at a lower altitude. The AE values corresponding to high AOD moment on high AOD days  
296 are extremely low ( $<0.5$ ), indicating that the particle size is large, thus, we suspect that these aerosols  
297 may consist of coarse sea salt particles.

## 298 **5 Summary**

299 This study analysed the AOD and AE variations retrieved from CE318-T sun photometer data spanning  
300 from January 2020 to April 2023 at Zhongshan Station in Antarctica. The main conclusions we draw are  
301 as follows:

302 AOD at Zhongshan Station ranged from 0.0 to 0.2, with fine mode particles concentrated in the low AOD  
303 range, and high AOD attributed to coarse mode particles.

304 AOD showed seasonal characteristics of low in summer, and high in winter, while AE showed the  
305 opposite. From spring to autumn, aerosols are dominated by fine particles, as retreating sea ice provides  
306 suitable conditions for phytoplankton blooms (Lizotte, 2001). In winter, the increase in sea salt  
307 dominated the increase in AOD and caused low AE levels. Additionally, summer and autumn AOD  
308 increases are possibly linked to particle growth, while spring and winter increases are associated with  
309 fine mode fraction decline.

310 Low aerosol load over Zhongshan Station was not enough to form an “aerosol-boundary layer” positive  
311 feedback mechanism, but the slight decrease in BLH may be related to AOD diurnal peak at 14:00.  
312 Moreover, high (low) wind speeds facilitated pollutant dispersion (accumulation), leading to reduced  
313 (increased) AOD. A weak positive correlation was noted between temperature and AOD ( $R = 0.22$ ,  $p =$   
314  $0.4$ ), and a negative correlation between relative humidity and AOD ( $R = -0.59$ ,  $p = 0.02$ ). The



315 mechanisms underlying temperature and humidity's influence on aerosols remain unclear, possibly  
316 linked to local aerosol properties at Zhongshan Station. In addition, we discuss the influence of aerosol  
317 sources on AOD. The backward trajectories show that the air masses on high AOD days come from the  
318 ocean, and the low AE values indicate that the particle size is larger, we speculate that the main  
319 composition of the aerosols is sea salt. The air masses on the low AOD days mainly come from the  
320 interior of Antarctica, and the high AE values indicate that the particle size is small. We speculate that  
321 the katabatic winds rush the air from the Antarctic plateau to Zhongshan Station.

#### 322 **Data availability**

323 The data included in this study can be accessed via <https://zenodo.org/records/10983098>. Boundary layer  
324 height data downloaded from ECMWF ERA5 ([https://www.ecmwf.int/en/forecasts/dataset/ecmwf-](https://www.ecmwf.int/en/forecasts/dataset/ecmwf-reanalysis-v5)  
325 [reanalysis-v5](https://www.ecmwf.int/en/forecasts/dataset/ecmwf-reanalysis-v5)). Backward trajectory of air mass and the meteorological data are obtained from NOAA  
326 Air Resources Laboratory ([https://www.ready.noaa.gov/HYSPLIT\\_traj.php](https://www.ready.noaa.gov/HYSPLIT_traj.php)).

#### 327 **Author contributions**

328 The paper is a result of the lead author's research work under the supervision of MD, LZ, YS. ZZ and  
329 YZ provided constructive comments. MD, QW and BT provided experimental data. ZL provided aerial  
330 photos of Zhongshan Station. LC wrote the first draft of the paper with the help and support of all the  
331 authors.

#### 332 **Competing interests**

333 The contact author has declared that none of the authors has any competing interests.

#### 334 **Acknowledgments**

335 Funding for this study was provided by the National Natural Science Foundation of China (42122047),  
336 the National Key Research and Development Program of China (2021YFC2802504), and the Basic  
337 Research Fund of the Chinese Academy of Meteorological Science (2023Z015&2023Z025).





338 **Reference**

339 Alghoul, M., Khamies, H., Assadeg, J., Yahya, M., Alfegi, E., and Sopian, K.:  
340 Impact of Aerosol Optical Depth on Solar Radiation Budget, in: Proceedings of the 3rd  
341 World Scientific and Engineering Academy and Society Int., Conference on renewable  
342 energy sources, 2009.

343 Altieri, K. E., Seitzinger, S. P., Carlton, A. G., Turpin, B. J., Klein, G. C., and  
344 Marshall, A. G.: Oligomers formed through in-cloud methylglyoxal reactions:  
345 Chemical composition, properties, and mechanisms investigated by ultra-high  
346 resolution FT-ICR mass spectrometry, *Atmospheric Environment*, 42, 1476–1490,  
347 <https://doi.org/10.1016/j.atmosenv.2007.11.015>, 2008.

348 Barreto, Á., Cuevas, E., Granados-Muñoz, M.-J., Alados-Arboledas, L., Romero,  
349 P. M., Gröbner, J., Kouremeti, N., Almansa, A. F., Stone, T., Toledano, C., Román, R.,  
350 Sorokin, M., Holben, B., Canini, M., and Yela, M.: The new sun-sky-lunar Cimel  
351 CE318-T multiband photometer - a comprehensive performance evaluation,  
352 *Atmospheric Measurement Techniques*, 9, 631–654, <https://doi.org/10.5194/amt-9-631-2016>, 2016.

354 Basharat, U., Tariq, S., Chaudhry, M. N., Khan, M., Bonah Agyekum, E., Fendzi  
355 Mbasso, W., and Kamel, S.: Seasonal correlation of aerosols with soil moisture,  
356 evapotranspiration, and vegetation over Pakistan using remote sensing, *Heliyon*, 9,  
357 e20635, <https://doi.org/10.1016/j.heliyon.2023.e20635>, 2023.

358 Boucher, O., Moulin, C., Belviso, S., Aumont, O., Bopp, L., Cosme, E., von  
359 Kuhlmann, R., Lawrence, M. G., Pham, M., Reddy, M. S., Sciare, J., and Venkataraman,  
360 C.: DMS atmospheric concentrations and sulphate aerosol indirect radiative forcing: a  
361 sensitivity study to the DMS source representation and oxidation, *Atmospheric  
362 Chemistry and Physics*, 3, 49–65, <https://doi.org/10.5194/acp-3-49-2003>, 2003.

363 Cecilia Arsene, Barnes, I., and Becker, K. H.: FT-IR product study of the photo-  
364 oxidation of dimethyl sulfide: Temperature and O<sub>2</sub> partial pressure dependence,  
365 *Physical Chemistry Chemical Physics*, 1, 5463–5470,  
366 <https://doi.org/10.1039/A907211J>, 1999.

367 Che, H., Xia, X., Zhao, H., Li, L., Gui, K., Zheng, Y., Song, J., Qi, B., Zhu, J.,  
368 Miao, Y., Wang, Y., Wang, Z., Wang, H., Dubovik, O., Holben, B., Chen, H., Shi, G.,  
369 and Zhang, X.: Aerosol optical and radiative properties and their environmental effects  
370 in China: A review, *Earth-Science Reviews*, 248, 104634,  
371 <https://doi.org/10.1016/j.earscirev.2023.104634>, 2024.

372 Coccia, M.: How do low wind speeds and high levels of air pollution support the  
373 spread of COVID-19?, *Atmos Pollut Res*, 12, 437–445,  
374 <https://doi.org/10.1016/j.apr.2020.10.002>, 2021.



- 375 Davison, B., O'dowd, C., Hewitt, C. N., Smith, M. H., Harrison, R. M., Peel, D.  
376 A., Wolf, E., Mulvaney, R., Schwikowski, M., and Baltenspergert, U.: Dimethyl sulfide  
377 and its oxidation products in the atmosphere of the Atlantic and Southern Oceans,  
378 Atmospheric Environment, 30, 1895–1906, [https://doi.org/10.1016/1352-](https://doi.org/10.1016/1352-2310(95)00428-9)  
379 2310(95)00428-9, 1996.
- 380 Ding, J., Dai, Q., Zhang, Y., Xu, J., Huangfu, Y., and Feng, Y.: Air humidity affects  
381 secondary aerosol formation in different pathways, Science of The Total Environment,  
382 759, 143540, <https://doi.org/10.1016/j.scitotenv.2020.143540>, 2021.
- 383 Ding, M., Zou, X., Sun, Q., Yang, D., Zhang, W., Bian, L., Lu, C., Allison, I., Heil,  
384 P., and Xiao, C.: The PANDA automatic weather station network between the coast and  
385 Dome A, East Antarctica, Earth System Science Data, 14, 5019–5035,  
386 <https://doi.org/10.5194/essd-14-5019-2022>, 2022.
- 387 Frey, M. M., Norris, S. J., Brooks, I. M., Anderson, P. S., Nishimura, K., Yang, X.,  
388 Jones, A. E., Nerentorp Mastromonaco, M. G., Jones, D. H., and Wolff, E. W.: First  
389 direct observation of sea salt aerosol production from blowing snow above sea ice,  
390 Atmospheric Chemistry and Physics, 20, 2549–2578, [https://doi.org/10.5194/acp-20-](https://doi.org/10.5194/acp-20-2549-2020)  
391 2549-2020, 2020.
- 392 Gabric, A. J., Shephard, J. M., Knight, J. M., Jones, G., and Trevena, A. J.:  
393 Correlations between the satellite-derived seasonal cycles of phytoplankton biomass  
394 and aerosol optical depth in the Southern Ocean: Evidence for the influence of sea ice,  
395 Global Biogeochemical Cycles, 19, <https://doi.org/10.1029/2005GB002546>, 2005.
- 396 Gadhavi, H. and Achuthan, J.: Aerosol characteristics and aerosol radiative forcing  
397 over Maitri, Antarctica, Current Sciece, 86, 296, 2004.
- 398 Gautam, S., Elizabeth, J., Gautam, A. S., Singh, K., and Abhilash, P.: Impact  
399 Assessment of Aerosol Optical Depth on Rainfall in Indian Rural Areas, Aerosol  
400 Science and Engineering, 6, 186–196, <https://doi.org/10.1007/s41810-022-00134-9>,  
401 2022.
- 402 Gobbi, G. P., Kaufman, Y. J., Koren, I., and Eck, T. F.: Classification of aerosol  
403 properties derived from AERONET direct sun data, Atmospheric Chemistry and  
404 Physics, 7, 453–458, <https://doi.org/10.5194/acp-7-453-2007>, 2007.
- 405 Hall, J. S. and Wolff, E. W.: Causes of seasonal and daily variations in aerosol sea-  
406 salt concentrations at a coastal Antarctic station, Atmospheric Environment, 32, 3669–  
407 3677, [https://doi.org/10.1016/S1352-2310\(98\)00090-9](https://doi.org/10.1016/S1352-2310(98)00090-9), 1998.
- 408 Han, D., Liu, W., Zhang, Y., Lu, Y., Liu, J., and Zhao, N.: Influence of temperature  
409 and relative humidity upon aerosol mass concentrations vertical distributions, Journal  
410 of University of Chinese Academy of Sciences, 24, 619,



- 411 <https://doi.org/10.7523/j.issn.2095-6134.2007.5.011>, 2007.
- 412 Harder, S., Warren, S. G., and Charlson, R. J.: Sulfate in air and snow at the South  
413 Pole: Implications for transport and deposition at sites with low snow accumulation,  
414 *Journal of Geophysical Research: Atmospheres*, 105, 22825–22832,  
415 <https://doi.org/10.1029/2000JD900351>, 2000.
- 416 Hennigan, C. J., Bergin, M. H., Dibb, J. E., and Weber, R. J.: Enhanced secondary  
417 organic aerosol formation due to water uptake by fine particles, *Geophysical Research*  
418 *Letters*, 35, <https://doi.org/10.1029/2008GL035046>, 2008.
- 419 Hong, J., Chen, L., and Yang, X.: Characteristics of the aerosols in Zhongshan  
420 Station, Antarctica (in Chinese), *Chinese Journal of Polar Research*, 21, 1, 2009.
- 421 Huang, Z., Ji, W., Yang, X., Huang, R., Tang, R., Yu, T., and Zhang, G.: The  
422 chemical composition of marine aerosol over Zhongshan Station in Antarctica and its  
423 sources discrimination in 1998 (in Chinese), *Acta Oceanologica Sinica*, 27, 59–66,  
424 2005.
- 425 Jurányi, Z. and Weller, R.: One year of aerosol refractive index measurement from  
426 a coastal Antarctic site, *Atmospheric Chemistry and Physics*, 19, 14417–14430,  
427 <https://doi.org/10.5194/acp-19-14417-2019>, 2019.
- 428 Kamra, V. P., Devendraa Siingh, A. K.: Antarctic Aerosols and Climate:  
429 Measurements at a Coastal Antarctic Station, in: *Climate Variability of Southern High*  
430 *Latitude Regions*, CRC Press, 2022.
- 431 Kang, S., Zhang, Y., Qian, Y., and Wang, H.: A review of black carbon in snow  
432 and ice and its impact on the cryosphere, *Earth-Science Reviews*, 210, 103346,  
433 <https://doi.org/10.1016/j.earscirev.2020.103346>, 2020.
- 434 Kannemadugu, H. B. S., Sudhakaran Syamala, P., Taori, A., Bothale, R. V., and  
435 Chauhan, P.: Atmospheric aerosol optical properties and trends over Antarctica using  
436 in-situ measurements and MERRA-2 aerosol products, *Polar Science*, 38, 101011,  
437 <https://doi.org/10.1016/j.polar.2023.101011>, 2023.
- 438 Kaufman, Y. J.: Aerosol optical thickness and atmospheric path radiance, *Journal*  
439 *of Geophysical Research: Atmospheres*, 98, 2677–2692,  
440 <https://doi.org/10.1029/92JD02427>, 1993.
- 441 Lachlan-Cope, T., Beddows, D. C. S., Brough, N., Jones, A. E., Harrison, R. M.,  
442 Lupi, A., Yoon, Y. J., Virkkula, A., and Dall'Osto, M.: On the annual variability of  
443 Antarctic aerosol size distributions at Halley Research Station, *Atmospheric Chemistry*  
444 *and Physics*, 20, 4461–4476, <https://doi.org/10.5194/acp-20-4461-2020>, 2020.



- 445 Li, J., Wang, W., Li, K., Zhang, W., Peng, C., Zhou, L., Shi, B., Chen, Y., Liu, M.,  
446 Li, H., and Ge, M.: Temperature effects on optical properties and chemical composition  
447 of secondary organic aerosol derived from *n*-dodecane, *Atmospheric Chemistry and*  
448 *Physics*, 20, 8123–8137, <https://doi.org/10.5194/acp-20-8123-2020>, 2020.
- 449 Li, J., Carlson, B. E., Yung, Y. L., Lv, D., Hansen, J., Penner, J. E., Liao, H.,  
450 Ramaswamy, V., Kahn, R. A., Zhang, P., Dubovik, O., Ding, A., Lacis, A. A., Zhang,  
451 L., and Dong, Y.: Scattering and absorbing aerosols in the climate system, *Nat Rev*  
452 *Earth Environ*, 3, 363–379, <https://doi.org/10.1038/s43017-022-00296-7>, 2022.
- 453 Liu, Y., Zhou, Y., and Lu, J.: Exploring the relationship between air pollution and  
454 meteorological conditions in China under environmental governance, *Sci Rep*, 10,  
455 14518, <https://doi.org/10.1038/s41598-020-71338-7>, 2020.
- 456 Lizotte, M. P.: The Contributions of Sea Ice Algae to Antarctic Marine Primary  
457 Production1, *American Zoologist*, 41, 57–73, <https://doi.org/10.1093/icb/41.1.57>, 2001.
- 458 Lou, M., Guo, J., Wang, L., Xu, H., Chen, D., Miao, Y., Lv, Y., Li, Y., Guo, X., Ma,  
459 S., and Li, J.: On the Relationship Between Aerosol and Boundary Layer Height in  
460 Summer in China Under Different Thermodynamic Conditions, *Earth and Space*  
461 *Science*, 6, 887–901, <https://doi.org/10.1029/2019EA000620>, 2019.
- 462 Meng, H., Bai, G., and Wang, L.: Analysis of the spatial and temporal distribution  
463 characteristics of AOD in typical industrial cities in northwest China and the influence  
464 of meteorological factors, *Atmospheric Pollution Research*, 15, 101957,  
465 <https://doi.org/10.1016/j.apr.2023.101957>, 2024.
- 466 Miao, Y. and Liu, S.: Linkages between aerosol pollution and planetary boundary  
467 layer structure in China, *Science of The Total Environment*, 650, 288–296,  
468 <https://doi.org/10.1016/j.scitotenv.2018.09.032>, 2019.
- 469 Pei, Q., Saikawa, E., Kaspari, S., Widory, D., Zhao, C., Wu, G., Loewen, M., Wan,  
470 X., Kang, S., Wang, X., Zhang, Y.-L., and Cong, Z.: Sulfur aerosols in the Arctic,  
471 Antarctic, and Tibetan Plateau: Current knowledge and future perspectives, *Earth-*  
472 *Science Reviews*, 220, 103753, <https://doi.org/10.1016/j.earscirev.2021.103753>, 2021.
- 473 Petäjä, T., Järvi, L., Kerminen, V.-M., Ding, A. J., Sun, J. N., Nie, W., Kujansuu,  
474 J., Virkkula, A., Yang, X., Fu, C. B., Zilitinkevich, S., and Kulmala, M.: Enhanced air  
475 pollution via aerosol-boundary layer feedback in China, *Sci Rep*, 6, 18998,  
476 <https://doi.org/10.1038/srep18998>, 2016.
- 477 Schuster, G. L., Dubovik, O., and Holben, B. N.: Angstrom exponent and bimodal  
478 aerosol size distributions, *Journal of Geophysical Research: Atmospheres*, 111,  
479 <https://doi.org/10.1029/2005JD006328>, 2006.



- 480 Shaw, G. E.: Considerations on the origin and properties of the Antarctic aerosol,  
481 *Reviews of Geophysics*, 17, 1983–1998, <https://doi.org/10.1029/RG017i008p01983>,  
482 1979.
- 483 Simmons, J. B., Humphries, R. S., Wilson, S. R., Chambers, S. D., Williams, A.  
484 G., Griffiths, A. D., McRobert, I. M., Ward, J. P., Keywood, M. D., and Gribben, S.:  
485 Summer aerosol measurements over the East Antarctic seasonal ice zone, *Atmospheric*  
486 *Chemistry and Physics*, 21, 9497–9513, <https://doi.org/10.5194/acp-21-9497-2021>,  
487 2021.
- 488 Sun, Y., Wang, Z., Fu, P., Jiang, Q., Yang, T., Li, J., and Ge, X.: The impact of  
489 relative humidity on aerosol composition and evolution processes during wintertime in  
490 Beijing, China, *Atmospheric Environment*, 77, 927–934,  
491 <https://doi.org/10.1016/j.atmosenv.2013.06.019>, 2013.
- 492 Thakur, R.: Trace elemental variability in aerosols near the two Indian Antarctic  
493 research stations during austral summer, No. 26, pp 61–74, 2019.
- 494 Thornhill, G., Collins, W., Olivie, D., Skeie, R. B., Archibald, A., Bauer, S., Checa-  
495 Garcia, R., Fiedler, S., Folberth, G., Gjernmunsen, A., Horowitz, L., Lamarque, J.-F.,  
496 Michou, M., Mulcahy, J., Nabat, P., Naik, V., O’Connor, F. M., Paulot, F., Schulz, M.,  
497 Scott, C. E., Séférian, R., Smith, C., Takemura, T., Tilmes, S., Tsigaridis, K., and Weber,  
498 J.: Climate-driven chemistry and aerosol feedbacks in CMIP6 Earth system models,  
499 *Atmos. Chem. Phys.*, 21, 1105–1126, <https://doi.org/10.5194/acp-21-1105-2021>, 2021.
- 500 Tian, B., Ding, M., Putero, D., Li, C., Zhang, D., Tang, J., Zheng, X., Bian, L., and  
501 Xiao, C.: Multi-year variation of near-surface ozone at Zhongshan Station, Antarctica,  
502 *Environ. Res. Lett.*, 17, 044003, <https://doi.org/10.1088/1748-9326/ac583c>, 2022.
- 503 Tomasi, C., Vitale, V., Lupi, A., Di Carmine, C., Campanelli, M., Herber, A.,  
504 Treffeisen, R., Stone, R. S., Andrews, E., Sharma, S., Radionov, V., von Hoyningen-  
505 Huene, W., Stebel, K., Hansen, G. H., Myhre, C. L., Wehrli, C., Aaltonen, V.,  
506 Lihavainen, H., Virkkula, A., Hillamo, R., Ström, J., Toledano, C., Cachorro, V. E.,  
507 Ortiz, P., de Frutos, A. M., Blindheim, S., Frioud, M., Gausa, M., Zielinski, T., Petelski,  
508 T., and Yamanouchi, T.: Aerosols in polar regions: A historical overview based on  
509 optical depth and in situ observations, *Journal of Geophysical Research: Atmospheres*,  
510 112, <https://doi.org/10.1029/2007JD008432>, 2007.
- 511 Tomasi, C., Lupi, A., Mazzola, M., Stone, R. S., Dutton, E. G., Herber, A.,  
512 Radionov, V. F., Holben, B. N., Sorokin, M. G., Sakerin, S. M., Terpigova, S. A.,  
513 Sobolewski, P. S., Lanconelli, C., Petkov, B. H., Busetto, M., and Vitale, V.: An update  
514 on polar aerosol optical properties using POLAR-AOD and other measurements  
515 performed during the International Polar Year, *Atmospheric Environment*, 52, 29–47,  
516 <https://doi.org/10.1016/j.atmosenv.2012.02.055>, 2012.



- 517 Udisti, R., Dayan, U., Becagli, S., Busetto, M., Frosini, D., Legrand, M., Lucarelli,  
518 F., Preunkert, S., Severi, M., Traversi, R., and Vitale, V.: Sea spray aerosol in central  
519 Antarctica. Present atmospheric behaviour and implications for paleoclimatic  
520 reconstructions, *Atmospheric Environment*, 52, 109–120,  
521 <https://doi.org/10.1016/j.atmosenv.2011.10.018>, 2012.
- 522 Virkkula, A., Grythe, H., Backman, J., Petäjä, T., Busetto, M., Lanconelli, C., Lupi,  
523 A., Becagli, S., Traversi, R., Severi, M., Vitale, V., Sheridan, P., and Andrews, E.:  
524 Aerosol optical properties calculated from size distributions, filter samples and  
525 absorption photometer data at Dome C, Antarctica, and their relationships with seasonal  
526 cycles of sources, *Atmospheric Chemistry and Physics*, 22, 5033–5069,  
527 <https://doi.org/10.5194/acp-22-5033-2022>, 2022.
- 528 Walters, W. W., Michalski, G., Böhlke, J. K., Alexander, B., Savarino, J., and  
529 Thiemens, M. H.: Assessing the Seasonal Dynamics of Nitrate and Sulfate Aerosols at  
530 the South Pole Utilizing Stable Isotopes, *Journal of Geophysical Research:  
531 Atmospheres*, 124, 8161–8177, <https://doi.org/10.1029/2019JD030517>, 2019.
- 532 Wang, X., Chen, L., Guo, K., and Liu, B.: Spatio-temporal trajectory evolution  
533 and cause analysis of air pollution in Chengdu, China, *Journal of the Air & Waste  
534 Management Association*, 72, 876–894,  
535 <https://doi.org/10.1080/10962247.2022.2058642>, 2022.
- 536 Weller, R. and Lampert, A.: Optical properties and sulfate scattering efficiency of  
537 boundary layer aerosol at coastal Neumayer Station, Antarctica, *Journal of Geophysical  
538 Research: Atmospheres*, 113, <https://doi.org/10.1029/2008JD009962>, 2008.
- 539 Weller, R., Wöltjen, J., Piel, C., Resenberg, R., Wagenbach, D., König-Langlo, G.,  
540 and Kriews, M.: Seasonal variability of crustal and marine trace elements in the aerosol  
541 at Neumayer station, Antarctica, *Tellus B*, 60, 742–752, [https://doi.org/10.1111/j.1600-  
0889.2008.00372.x](https://doi.org/10.1111/j.1600-<br/>542 0889.2008.00372.x), 2008.
- 543 Weller, R., Schmidt, K., Teinilä, K., and Hillamo, R.: Natural new particle  
544 formation at the coastal Antarctic site Neumayer, *Atmospheric Chemistry and Physics*,  
545 15, 11399–11410, <https://doi.org/10.5194/acp-15-11399-2015>, 2015.
- 546 Xu, G., Chen, L., Zhang, M., Zhang, Y., Wang, J., and Lin, Q.: Year-round records  
547 of bulk aerosol composition over the Zhongshan Station, Coastal East Antarctica, *Air  
548 Qual Atmos Hlth*, 12, 271–288, <https://doi.org/10.1007/s11869-018-0642-9>, 2019.
- 549 Xu, G., Chen, L., Xu, T., He, S., and Gao, Y.: Distributions of water-soluble ions  
550 in size-aggregated aerosols over the Southern Ocean and coastal Antarctica, *Environ.  
551 Sci.: Processes Impacts*, 23, 1316–1327, <https://doi.org/10.1039/D1EM00089F>, 2021.
- 552 Yan, J., Jung, J., Lin, Q., Zhang, M., Xu, S., and Zhao, S.: Effect of sea ice retreat



553 on marine aerosol emissions in the Southern Ocean, Antarctica, *Sci Total Environ*, 745,  
554 140773, <https://doi.org/10.1016/j.scitotenv.2020.140773>, 2020.

555 Yang, Y., Zhao, C., Wang, Q., Cong, Z., Yang, X., and Fan, H.: Aerosol  
556 characteristics at the three poles of the Earth as characterized by Cloud–Aerosol Lidar  
557 and Infrared Pathfinder Satellite Observations, *Atmospheric Chemistry and Physics*, 21,  
558 4849–4868, <https://doi.org/10.5194/acp-21-4849-2021>, 2021.

559 Yu, L., Zhong, S., and Sun, B.: The Climatology and Trend of Surface Wind Speed  
560 over Antarctica and the Southern Ocean and the Implication to Wind Energy  
561 Application, *Atmosphere*, 11, 108, <https://doi.org/10.3390/atmos11010108>, 2020.

562 Zhang, F.: Factors Influencing the Spatio–Temporal Variability of Aerosol Optical  
563 Depth over the Arid Region of Northwest China, *Atmosphere*, 15, 54,  
564 <https://doi.org/10.3390/atmos15010054>, 2024.

565 Zhang, M., Chen, L., Xu, G., Lin, Q., and Liang, M.: Linking Phytoplankton  
566 Activity in Polynyas and Sulfur Aerosols over Zhongshan Station, East Antarctica,  
567 *Journal of the Atmospheric Sciences*, 72, 4629–4642, [https://doi.org/10.1175/JAS-D-](https://doi.org/10.1175/JAS-D-15-0094.1)  
568 15-0094.1, 2015.

569